# Potential of the Bi-Static SAR Satellite Companion Mission Harmony for Land-Ice Observations

Kääb, Andreas; Mouginot, Jérémie; Prats-Iraola, Pau; Rignot, Eric; Rabus, Bernhard; Benedikter, Andreas; Rott, Helmut; Nagler, Thomas; Rommen, Björn; Lopez-Dekker, Paco

**DOI**
10.3390/rs16162918

**Publication date**
2024

**Document Version**
Final published version

**Published in**
Remote Sensing

**Citation (APA)**
Kääb, A., Mouginot, J., Prats-Iraola, P., Rignot, E., Rabus, B., Benedikter, A., Rott, H., Nagler, T., Rommen, B., & Lopez-Dekker, P. (2024). Potential of the Bi-Static SAR Satellite Companion Mission Harmony for Land-Ice Observations. *Remote Sensing*, *16*(16), Article 2918. https://doi.org/10.3390/rs16162918

*remote sensing*

MDPI

*Article*

# Potential of the Bi-Static SAR Satellite Companion Mission Harmony for Land-Ice Observations

**Andreas Kääb [1,*], Jérémie Mouginot [2,†], Pau Prats-Iraola [3], Eric Rignot [4], Bernhard Rabus [5], Andreas Benedikter [3], Helmut Rott [6], Thomas Nagler [6], Björn Rommen [7] and Paco Lopez-Dekker [8]**

1 Department of Geosciences, University of Oslo, 0316 Oslo, Norway
2 Institute of Environmental Geosciences, University Grenoble Alpes, 38000 Grenoble, France
3 Microwaves and Radar Institute, German Aerospace Center, 82234 Wessling, Germany
4 Department of Earth System Science, University of California Irvine, Irvine, CA 92617, USA
5 School of Engineering Science, Simon Fraser University, Burnaby, BC V5A 1S6, Canada
6 ENVEO Environmental Earth Observation IT GmbH, 6020 Innsbruck, Austria
7 European Space Agency (ESA-ESTEC), 2200 Noordwijk, The Netherlands
8 Department of Geoscience and Remote Sensing, Delft University of Technology, 2628 Delft, The Netherlands
* Correspondence: kaeaeb@geo.uio.no
† Deceased.

**Abstract:** The EarthExplorer 10 mission Harmony by the European Space Agency ESA, scheduled for launch around 2029–2030, consists of two passive C-band synthetic-aperture-radar companion satellites flying in a flexible constellation with one Sentinel-1 radar satellite as an illuminator. Sentinel-1 will serve as transmitter and receiver of radar waves, and the two Harmonys will serve as bistatic receivers without the ability to transmit. During the first and last year of the 5-year mission, the two Harmony satellites will fly in a cross-track interferometric constellation, such as that known from TanDEM-X, about 350 km ahead or behind the assigned Sentinel-1. This constellation will provide 12-day repeat DEMs, among other regions, over most land-ice and permafrost areas. These repeat DEMs will be complemented by synchronous lateral terrain displacements from the well-established offset tracking method. In between the cross-track interferometry phases, one of the Harmony satellites will be moved to the opposite side of the Sentinel-1 to form a symmetric bistatic "stereo" constellation with ±~350 km along-track baseline. In this phase, the mission will provide opportunity for radar interferometry along three lines of sight, or up to six when combining ascending and descending acquisitions, enabling the measurement of three-dimensional surface motion, for instance sub- and emergence components of ice flow, or three-dimensional deformation of permafrost surfaces or slow landslides. Such measurements would, for the first time, be available for large areas and are anticipated to provide a number of novel insights into the dynamics and mass balance of a range of mass movement processes.

**Keywords:** synthetic aperture radar; bi-static; multi-static; satellite constellation



**Citation:** Kääb, A.; Mouginot, J.; Prats-Iraola, P.; Rignot, E.; Rabus, B.; Benedikter, A.; Rott, H.; Nagler, T.; Rommen, B.; Lopez-Dekker, P. Potential of the Bi-Static SAR Satellite Companion Mission Harmony for Land-Ice Observations. *Remote Sens.* **2024**, *16*, 2918. https://doi.org/10.3390/rs16162918

Academic Editor: Peter Romanov

Received: 28 June 2024
Revised: 6 August 2024
Accepted: 7 August 2024
Published: 9 August 2024



## 1. Introduction

Synthetic aperture radar (SAR) from satellites is a key method to map and monitor the properties of and changes in Earth's cryosphere [1]. SAR backscatter analysis and SAR interferometry have become indispensable to map glacier, ice sheet, and rock glacier velocities [2–5]; ice sheet grounding lines [6]; sea-ice conditions and drift [7,8]; snow cover [9–12]; lowland permafrost changes and deformation [13,14]; and other cryospheric processes, e.g., river ice, lake ice, and landslides. In particular, the operational Copernicus Sentinel-1 constellation, consisting of two monostatic SAR satellites (currently only Sentinel-1A is operational after the failure of 1B in December 2021), and its freely available data policy have boosted cryospheric applications of SAR. Bi- and multi-static SAR missions, i.e., missions where a radar transmitter and two or more receivers, respectively, are at different

positions, have extended cryospheric SAR applications significantly [15]. Well-known examples for bistatic SAR missions are the Shuttle Radar Topography Mission (SRTM) and TanDEM-X. They provide(d) not least interferometric elevation measurements during a single overpass, avoiding phase decorrelation problems and mitigating the impact of the atmosphere, thus revolutionizing the availability and application of (near-) global high-resolution digital elevation models (DEMs) [16,17]. At the same time, bistatic SAR configurations maintain the ability of monostatic SAR to perform repeat-pass interferometry or offset tracking to measure surface displacements over a range of magnitudes.

In this contribution, we present the forthcoming multi-static SAR satellite mission "Harmony" and its potential applications on ice sheets, glaciers, and permafrost. The European Space Agency (ESA) Earth Explorers with, for instance, the radar altimeter CRYOSAT-2, the gravity mission GOCE, or the soil moisture and ocean salinity mission SMOS, are a series of science-driven Earth-observation satellite missions. The Harmony mission has been down-selected in summer 2022 to be ESA's Earth Explorer 10 (EE10) mission to be further developed and launched around 2029. In the following, we present Harmony's science goals, the mission concept, and then in more detail, we describe individual novel measurements expected from the mission for land cryosphere. Our contribution is in part based on the mission justification and implementations as presented in Harmony's Report for Mission Selection [18].

Below we list the nominal scientific goals and objectives of Harmony. It is important to stress that the Harmony mission also has, besides its goals regarding ice sheets, glaciers, and permafrost, a number of other key goals related to oceans, sea ice, and solid Earth [18], making Harmony a broad Earth System Observatory mission rather than a narrow topical mission. On the other hand, these multiple goals and objectives need to be balanced within the mission concept, sometimes requiring compromises regarding instrument design, measurement concepts, and acquisition priorities.

Harmony's overall scientific goals regarding land ice [19] (Table 1, Figure 1) are improved quantification and understanding of the following:

- mass balance of grounded ice sheets, ice caps and glaciers, their relative contributions to global sea-level change, their current stability, and their sensitivity to climate change;
- changes taking place in permafrost and frozen-ground regimes, their feedback to climate system and terrestrial ecosystems.

Harmony's primary objectives for land ice to contribute to the above goals are to

- provide a consistent and highly resolved global glacier mass balance, filling major spatial gaps in the current observation of mountain glaciers and ice sheets (details in Sections 3 and 4);
- give new insights into the coupling between glacier mass change and ice dynamics, and through that, improve understanding of rapid glacier changes, and the balance between three-dimensional ice motion and mass accumulation/ablation (Section 5.1).

A secondary objective for land ice, i.e., an objective with reduced priority regarding instrument design, measurement concept, and acquisition plan, is to

- provide large-area information on the spatial distribution, extent, and magnitude of heave/subsidence and erosion in permafrost areas (Section 5.2).

In addition to these nominal land-ice-related mission goals and objectives, a number of other more explorative applications will be investigated during the mission preparation and lifetime (examples in Section 6).

For a short overview, the key goals of the Harmony mission concerning solid Earth, ocean, and ocean–atmosphere dynamics include the following [18]: map three components of global tectonic strain and the deformation caused by volcanism and the earthquake cycle; better understand cycles of topographic evolution at active volcanoes; quantify and disentangle air–sea interactions and adjustment between ocean features and the marine atmospheric boundary layer [20]; improve the understanding of tropical and intense extratropical cyclones; resolve the upper ocean deformation in order to understand its

contribution to ocean circulation, ventilation, heat uptake, CO2 sequestration, water cycle, and vertical ocean transport processes; measurements of instantaneous sea-ice velocities to better understand sea-ice dynamics, and improve sea-ice rheological models [21].

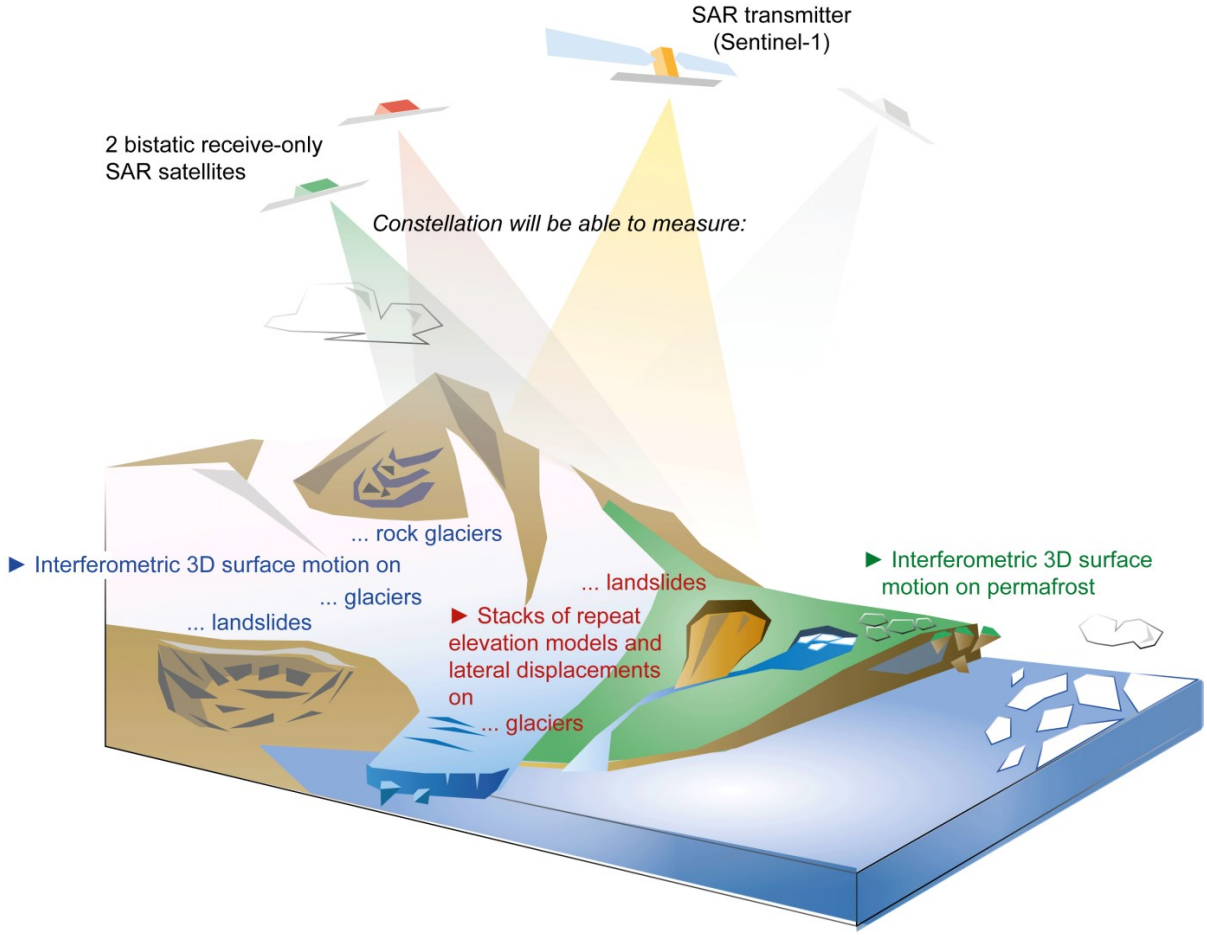


**Figure 1.** Graphical summary of Harmony land-ice measurement objectives.

**Table 1.** Overview of Harmony's scientific mission goals and objectives related to land ice, measurements, and main spatial focus.

| | |
|---|---|
| **Scientific goals [19]:** | Improved mass balance of glaciers and ice sheets; contribution to global sea level rise; stability and sensitivity; changes in permafrost |
| **Scientific objectives:** | - consistent and highly resolved global glacier mass balance;<br>- filling major spatial gaps in the current observation of mountain glaciers and ice sheets;<br>- coupling between glacier mass change and ice dynamics, and through that, improve understanding of rapid glacier changes, and the balance between vertical ice flow and mass accumulation/ablation;<br>- large-area information on the spatial distribution, extent and magnitude of heave/subsidence and erosion in permafrost areas |

| Measurement Objectives | Configuration/Method Used | Intermediate Products | Mission Years | Requirements (Resolution, Accuracy) | Land-Ice Focus |
|---|---|---|---|---|---|
| Elevation changes over 5 years | Cross-track interferometry | Stacks of DEMs with 12-day repeat | 1 + 5 | $100 \times 100$ m$^2$ $\pm$ 0.5 m/yr (threshold, T) $50 \times 50$ m$^2$ $\pm$ 0.2 m/yr (goal, G; $30 \times 30$ m$^2$ for permafrost) | Glaciers, ice-sheet margins, permafrost |

**Table 1.** *Cont.*

| | | | | | |
|---|---|---|---|---|---|
| Seasonal elevation changes | Cross-track interferometry | Stacks of DEMs with 12-day repeat | 1 + 5 | " | Glaciers, ice-sheet margins, landslides |
| Simultaneous elevation changes and lateral displacements | Cross-track interferometry; combined with offset tracking | Stacks of DEMs with 12-day repeat + lateral offsets between repeat SAR data | 1 + 5 (displacements only: 2–4) | " | Glaciers, ice-sheet margins, landslides |
| Three-dimensional surface deformation | Stereo; using repeat-pass interferometry | 12-day line-of-sight displacements in multiple directions | 1–5, with larger LoS-diversity during 2–4 | $100 \times 100$ m$^2$ $\pm$ 5% (threshold, T) $30 \times 30$ m$^2$ $\pm$ 3% m/yr (goal, G) | Glaciers and ice sheets outside melting season; permafrost, rock glaciers, slow landslides |

## 2. Mission Concept

Harmony's mission concept consists of two C-band receive-only, i.e., passive, SAR satellites flying in a configurable convoy formation with one Sentinel-1 satellite (status 2024: likely Sentinel-1D), which will be used as a radar illuminator (Figures 1 and 2). Harmony will thus provide Sentinel-1-like but bi-static SAR data. In addition to the radar, the two Harmony satellites will also carry a thermal infrared (TIR) camera system providing several simultaneous observations of the radar swath at different along-track viewing angles. The data from the TIR payload with ground resolutions between 300 m (pan) and 1 km (TIR bands) are meant to retrieve sea-surface temperatures (SST) and cloud heights and cloud motion over the ocean and are not further discussed here.

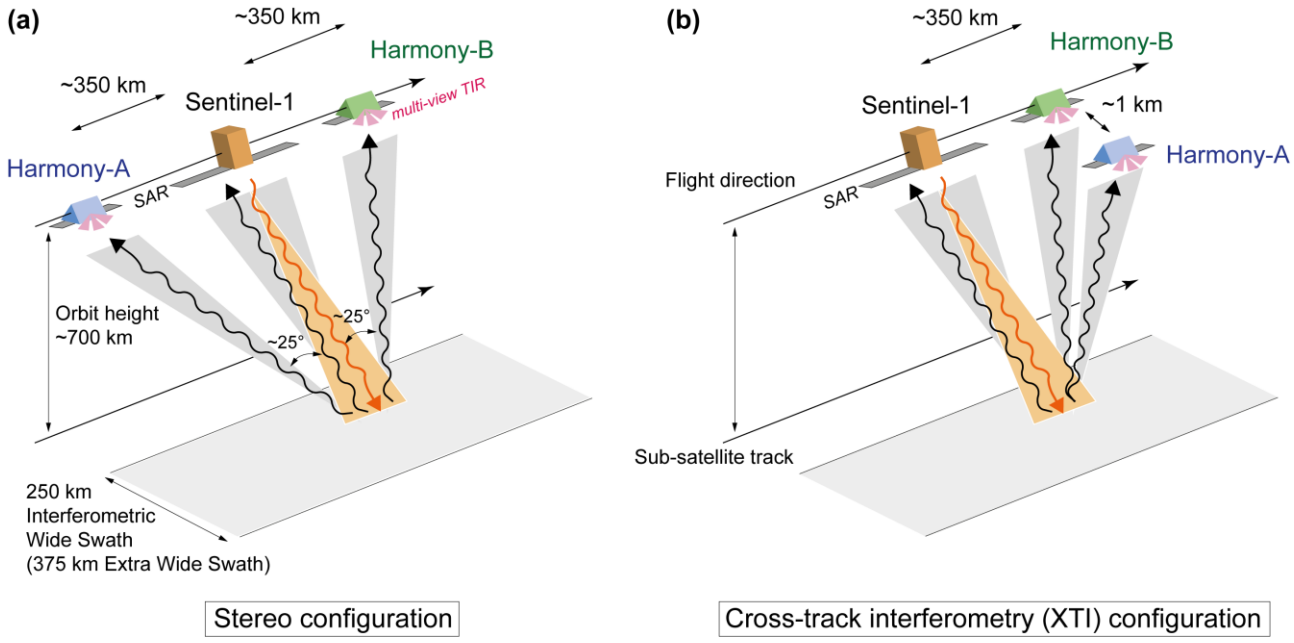


**Figure 2.** The Harmony mission consists of two satellites with one passive SAR instrument each, Harmony-A and Harmony-B. They will fly in two alternating configurations in convoy with Sentinel-1, which serves as a radar transmitter for the two receive-only Harmony satellites. (**a**) The stereo configuration is optimized to measure surface motion vectors on land and ocean and is foreseen for years 2–4 of the mission. (**b**) The cross-track interferometric (XTI) configuration is optimized to measure land surface topography every 12 days during years 1 and 5.

Two different configurations of the two Harmony satellites are foreseen:

- A "stereo" configuration, optimized for the measurement of motion vectors, where each Harmony satellite is positioned on either side in the along-track direction of Sentinel-1 with a separation distance in the order of 300–400 km (to be optimized for performance but kept constant in orbit) (Figure 2a).

- An "across-track interferometry" (XTI) configuration, optimized for the single-pass interferometric measurement of time series of surface topography, where one of the Harmony satellites will be positioned in a close formation (several hundred meters cross-track separation; baseline) with the other Harmony satellite, similar to the TanDEM-X mission (Figure 2b). Additionally, in this phase, the along-track separation distance between the close XTI-formation of both Harmony satellites and Sentinel-1 will remain in the order of 300–400 km.

Repeat-pass Interferometric Synthetic Aperture Radar (InSAR) using three different lines of sight (LoS), one from Sentinel-1 and two for the two Harmony satellites, will provide high sensitivity for along-track and cross-track surface deformation components. Combining ascending and descending passes will then allow the measurement of fully three-dimensional (3D) interferometric surface motions (Section 5). Repeat-pass interferometry requires phase coherence over the repeat time (12 days or a multiple for Harmony) and will therefore be mainly successful over lowland and mountain permafrost; over polar glaciers and ice sheets outside of the melting season; rock glaciers and slow landslides; and not least, but not further discussed here, for solid Earth applications, such as tectonic deformations.

During the single-pass XTI mission phases, Harmony will be able to generate time series of Digital Elevation Models (DEMs) in a similar way to TanDEM-X (Sections 3 and 4). Three-dimensional surface deformation measurements will still be possible during the XTI phases, though based on two significantly diverse lines of sight instead of three as for the stereo phase: one for Sentinel-1 and one for the close formation of the two Harmony satellites (Section 5).

During the nominal mission lifetime of 5 years, the close-formation XTI phases of one full year each would be conducted in the first year, year 1, and the last year, year 5. The stereo phase would last at least two consecutive years, with the possibility for constellation reformation to allow for occasional XTI observations (Table 1). Additional intermediate short XTI phases during the stereo phase are under consideration.

As the two Harmony satellites will only be able to accompany one of the Sentinel-1 satellites, the repeat time of the mission will be the same as for one Sentinel-1 satellite, namely 12 days. Furthermore, Harmony will only be able to acquire data when this Sentinel-1 satellite is transmitting so that the Sentinel-1 and Harmony acquisitions plans are coordinated. The passive SARs onboard the two companion satellites will be able to acquire data from all Sentinel-1 sub-swaths and all their modes: Interferometric Wide swath mode (IW; most relevant for land-ice applications); Extra Wide swath mode (EW; relevant for sea-ice applications but also for polar glaciers), Stripmap Mode (SM); and Wave Mode (WV). Like Sentinel-1, the passive SARs will be able to acquire two orthogonal polarizations simultaneously.

Being dependent on one Sentinel-1 satellite as transmitter, the Harmony mission would be affected by changes or problems of the Sentinel-1 mission. Sentinel-1C is planned to launch in late 2024 (status summer 2024) with a nominal lifetime that would not or only slightly overlap with the Harmony mission. The latter is thus planned to fly together with Sentinel-1D. The Harmony mission is currently technologically designed to work with the first-generation Sentinel-1 satellites (1A–1D) but would not be fully technologically compatible with the much-changed Sentinel-1 next-generation (NG) satellites currently under planning. However, the Sentinel-1 NG satellites are currently required to have a legacy mode that would make them compatible with Harmony, at least for dedicated measurement campaigns.

Planned Level-1 land-ice products for the mission include single-look complex data for the two Harmony satellites and co-registered single-look complex data of the mothership Sentinel-1 and the two Harmony satellites. Planned Level-2 products for land ice include single-pass XTI interferograms, derived digital surface models and topographic change between them. A second stream of Level-2 products is planned for stereo- and XTI-mode interferometric velocities over 12 days (and perhaps longer time intervals) between

repeat single-pass data and time series of these. A third stream of Level-2 products, temporal offsets from amplitude or speckle tracking over 12 days (and perhaps longer) between repeat data from Harmony A, Harmony B, and Sentinel-1, respectively, is under consideration. At Level 3, these products are then the base for spatio-temporal topographic change, three-dimensional surface velocities, and time series of these.

## 3. Global Multi-Year Glacier Elevation Changes

### *3.1. Glacier DEMs*

Comparing multi-temporal DEMs is a well-established method to estimate glacier volume and mass changes [22]. Glacier-elevation-change studies typically cover local to regional scales and often rely on a heterogeneous spatio-temporal patchwork of different data sets with different time stamps and characteristics [23]. Many glaciers are small, so that only high-resolution data have the potential for complete survey of glaciers on Earth. Globally consistent and highly resolved data sets of glacier elevation and elevation change in regular (decadal, by order of magnitude) time intervals are much needed to reduce uncertainty levels of global glacier volume and mass change, as well as its projections. Hugonnet et al. [24] provide the first and, so far, only highly resolved global glacier elevation trends from 20 years of ASTER optical satellite stereo DEMs. The latter study represents a milestone in mapping global glacier change but has a temporal resolution of only about 5–10 years, suffers from cloud cover in several regions, and has limited accuracy particularly in accumulation areas where low-visual-contrast hampers stereo parallax matching. The ASTER sensor is currently being phased out so that this time series cannot be continued.

Other (near-)global DEMs over glaciers are produced from SRTM data (60°N to 56°S), TanDEM-X data, or large-scale very-high-resolution optical satellite stereo data [22]. These DEMs form important benchmarks for regional to global glacier volume changes, with method-specific advantages and limitations, related, for instance, to incomplete coverage, inconsistent time stamps, or radar penetration bias. Radar (CryoSat-2) or lidar satellite altimetry (ICESat, ICESat-2) data have major gaps in regions of complex topography [25–28].

The Harmony mission aims to provide globally comprehensive and spatially detailed measurements of glacier surface elevation changes over well-defined epochs. Over the ice sheets, the mission will focus on outlet glaciers and areas of complex topography. The concept is to compare dense time series of interferometric DEMs (as few as 12 days repeat) generated during the full-year XTI phases in mission years 1 and 5 to estimate 5-year glacier elevation changes globally (Figure 3). The fact that the mission's 5-year elevation changes can be based on two full-year stacks of DEMs enables a versatile estimation of differences, such as from full-year averages, seasonal averages, single DEMs, or DEMs selected based on accuracy indicators. Harmony's year 1 or 5 annual glacier DEM stacks can also be compiled to reference DEMs to be compared against earlier DEMs (e.g., SRTM, TanDEM-X, ASTER, WorldView, CryoSat-2, ICESat) and to complement future elevation missions, potentially flying end 2020s to mid-2030s [22].

Harmony's XTI-DEMs are planned to have spatial resolutions of between 50 m and 100 m (depending on the spatial averaging, multi-looking, to be applied), with standard deviations of single DEM elevations of in general 1–3 m, depending on glacier facies and conditions, and on perpendicular baselines of the XTI-formation (Figure 4). For dry snow with large penetration depths, an elevation accuracy of a maximum 4–5 m is expected. As such accuracies for single DEMs are useful only for DEM comparisons over longer time scales (decadal and more) or for comparably large elevation changes, the targeted sub-meter accuracy of the 5-year glacier elevation changes within the Harmony lifetime will require special attention to penetration bias (see below section).

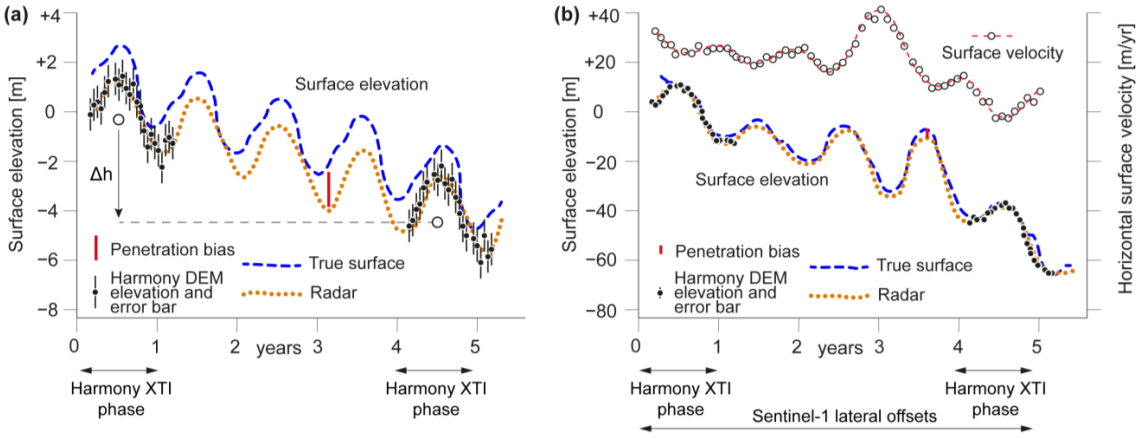


**Figure 3.** Schematics of Harmony time series for the cases of (**a**) small elevation changes (few meters over several months to years) and of (**b**) large elevation changes (tens of meters) for a hypothetical glacier point. (**b**) shows combined elevation changes and horizontal speeds. During the full mission years 1 and 5, Harmony is foreseen to measure dozens of DEMs over glaciers and ice-sheet margins globally (black points with error bars). The blue and brown curves indicate hypothetical idealized glacier elevation variations over time. Note that the vertical axes of panel (**a**,**b**) have scales that are different by an order of magnitude. (**a**) The mission will be able to deliver glacier volume changes Δh from differencing the DEM stacks from years 1 and 5. For small glacier thickness changes, the penetration bias between real surface and a radar-interferometric DEM is substantial, relative to the expected elevation changes, and needs to be dealt with. (**b**) Harmony's repeat DEMs, potentially combined with lateral surface displacements from radar offset tracking, can be used to study the interplay between changes in ice dynamics and ice thickness, such as for calving glaciers or glacier surges. Compared to the large elevation changes expected for such cases, radar penetration and DEM errors are relatively small and of less concern than in case (**a**).

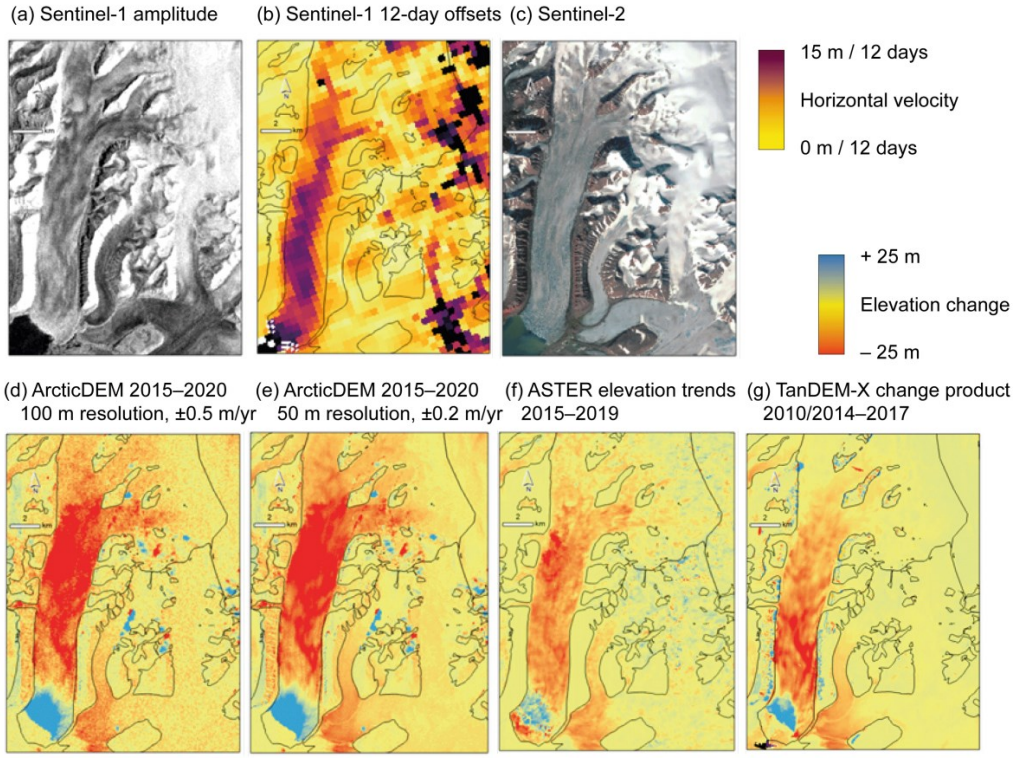


**Figure 4.** Visualization and comparison of some expected Harmony results using Tunabreen (78.46°N, 17.4°E), Svalbard, as an example. (**a**) Sentinel-1 amplitude image (gamma0, 12 March 2020).

(**b**) Sentinel-1 12-day offsets over 19–31 January 2019. (**c**) Sentinel-2 image (infrared false color, for orientation only, 2 August 2019). (**d**) Elevation differences from Arctic-DEM [29] strips of 17 March 2015 and a mosaic of 11 and 15 March 2020 resampled to 100 m resolution with random noise of ±0.5 m/yr added. (**e**) Same as (**d**), but resampled to 50 m and with ±0.2 m/yr noise added. (**f**) Elevation trends from ASTER stacks 2015–2019 [24]. (**g**) TanDEM-X topographic change product, computed between TanDEM-X elevations compiled over 2010–2014 and elevations from 2017. Note, panels (**d**,**e**) are visualizations (not simulations) of Harmony XTI 5-year DEM differences for the threshold (panel (**d**)) and goal requirements (panel (**e**)). They do not include potential errors from SAR XTI processing (e.g., steep terrain, penetration), but rather errors from optical stereo processing (e.g., small clouds, lack of visual contrast). Black glacier outlines are from Randolph glacier inventory v7. Note also that the ASTER DEM differences are just shown for visual comparison, and that the potential reasons for the differences between the DEM differences from ASTER and Arctic-DEM are not the subject of the present contribution.

### *3.2. Penetration Bias in DEMs*

The XTI method to be used by Harmony to measure glacier DEMs is well-demonstrated by the TanDEM-X mission. However, even more than for the X-band radar of TanDEM-X, the elevation bias due to the penetration of the C-band radar waves into snow and firn is considered to be a major source for surface elevation and geolocation error and bias [25,30–34] (Figure 3a). The following strategies are envisaged to minimize the influence of or correct for the elevation bias due to radar penetration in Harmony DEMs over snow and firn, respectively:

- estimation of the penetration length from the interferometric coherence according to Dall [35] and computation of the associated DEM and geolocation bias;
- comparison of interferometric DEMs from different incidence angles. The penetration length and the resulting DEM bias are dependent on the radar incidence angle. For stable snow and firn conditions and thus stable penetration bias (which in turn can be assessed from radar backscatter), penetration bias can be estimated from overlapping DEMs acquired from neighboring orbits. This method will not be available everywhere and at any time but could provide spatio-temporal samples of elevation biases to complement the other approaches;
- the two full-year time series of roughly bi-weekly DEMs from the same reference orbit (Figure 3a), and more frequent DEMs when combining DEMs from ascending and descending and neighboring orbits, can not only be used to increase elevation accuracy by DEM stacking, but also to analyze the seasonal cycle and weather dependence of elevation bias, for instance, by identifying sudden elevation jumps in space and time due to changes in penetration. The impact of radar penetration bias on Harmony's 5-year elevation changes can be reduced by selecting similar snow and firn conditions, and thus similar penetration conditions, in the DEM time series of both years 1 and 5. In principle, the elevation differences between the DEM stacks of years 1 and 5 are not fully affected by elevation bias due to penetration but only the (smaller) differential bias between these two years.
- All the above approaches can be combined. Independent validation is foreseen using elevation measurements from, for instance, optical satellite stereo data, altimetric missions (e.g., the Ku-band and Ka-band CRISTAL mission), or airborne laser scanning [30,31,33,36–38].

Despite the above approaches, it is clear that the elevation uncertainties associated with the penetration of the radar signals into snow and firn, together with the uncertainties from temporal variations in firn compaction, can reach the same order of magnitude as the actual elevation changes in glacier accumulation areas. For large (sub-)seasonal glacier elevation changes, such as in glacier ablation areas, from glacier surges, or at calving fronts (Section 4; Figure 3b), the effect of radar penetration is considered small both in absolute terms (little penetration into ice) and relative terms (elevation changes >> penetration bias).

## 4. Sub-Seasonal Elevation Changes and Simultaneous Glacier Velocities

In addition to the long-term integrated adjustment to climate changes (Section 3), the Harmony mission will also observe more rapid glacier changes, typically caused by dynamic responses of glaciers to external and internal forcings. Surges and glacier avalanches are expressions of such abrupt responses [39–42]. Large seasonal fluctuations in ice dynamics have been shown to correlate with significant dynamic thinning or thickening of tidewater glaciers [43]. The physical mechanisms associated with these large seasonal dynamic changes are still little understood. The dense global glacier DEM series provided by the Harmony mission during its years 1 and 5 will enable detecting and investigating such large short-term elevation changes. The DEM errors and potential penetration elevation bias (Section 3) in the order of meters are thereby of reduced concern (Figure 3b).

A specific and unique advantage of Harmony is the possibility to measure lateral displacements simultaneously to elevation changes (Figures 3b and 4). For the last decades, repeat SAR satellite data have been successfully used to map glacier flow independent of cloud cover, solar illumination, or the presence of distinct visual surface features. Today, satellite SAR offset tracking, repeat-pass radar interferometry, or optical feature tracking are standard techniques for measuring ice movement and, combined with ice thickness, to derive ice discharge, into the ocean [5,44–47].

Many important and fast ice sheet and glacier elevation changes are actually driven by changes in ice dynamics and ice discharge, rather than the often more gradual climate-driven mass change. Mass changes in the Greenland ice sheet are mainly due to a combination of changes in surface mass balance and ice dynamics, and for the Antarctic ice sheet, it is mainly due to changes in ice dynamics. While surface mass balance dominates typically the long-term mass change for mountain glaciers, ice dynamics can control strong elevation changes over shorter time scales, such as during glacier surges or calving front retreats. This all implies that the integration of measurements of lateral ice flow and simultaneous elevation changes holds a large potential to understand and predict fast glacier volume losses. Today, the only missions available to perform such simultaneous measurements of lateral displacement and elevation change are TanDEM-X and optical stereo missions and combinations [39,40,43,48]. Both types of mission demonstrated the large potential of combining lateral displacements and elevation change over glaciers but are feasible only over a few selected study sites. Otherwise, conclusions about the coupling between ice dynamics and thickness change have to be drawn from temporally often highly disconnected separate measurements of glacier flow and thickness change, whereby the main bottleneck stems in particular from the lack of elevations with a temporal repeat frequency in the same order of magnitude than the lateral displacements.

Combining the frequent Harmony single-pass interferometric DEMs during years 1 and 5 with offset tracking between repeat Sentinel-1 or Harmony single-look complex data (i.e., consisting of amplitude and phase of the radar backscatter) to measure ice displacements and large elevation changes, both in the order of several meters or tens of meters over days to weeks, routinely provides simultaneous, global-scale and frequent lateral displacements and elevation changes. In addition, Harmony's XTI mode would also have the advantage of providing the exact topographic component in range offset or phase, where current observations have to rely on external digital elevation models to account for topographic effects. As a result, the ice displacement measured through Harmony could be more accurate than from Sentinel-1 alone and could also resolve three-dimensional surface motion [49]. Harmony will thus also facilitate partitioning the mass loss of calving glaciers into components due to ice dynamics and surface mass balance, which both are the main drivers that need to be known to estimate the future evolution of the ice sheets.

## 5. Three-Dimensional Surface Velocities

Radar interferometry with two diverse lines of sight has so far only been possible when combining measurements from ascending and descending orbit tracks, with three diverse lines of sight only in rare cases when combination of coherent phase data from two different

ascending and one descending orbit tracks, or vice versa, are available. Furthermore, the lines of sights of past and current SAR sensors are perpendicular to flight direction, making SAR systems over lower latitudes much more sensitive to ground movements in the East–West direction than to those in the North–South direction. Both current limitations are overcome by the Harmony mission, making its ability to measure three-dimensional surface displacements interferometrically to one of Harmony's most novel aspects.

### *5.1. Submergence, Emergence, and Short-Term Deformations at Glacier Surface*

The method of combining Harmony's glacier elevation changes from repeat single-pass interferometry with simultaneous lateral displacements from offset tracking as described in Section 4 does not require interferometric phase coherence between the acquisitions dates as it can be based on features of backscatter magnitude only [49–51]. In fact, the large changes associated with the latter method typically lead to phase decorrelation. Where phase coherence is, however, maintained between Harmony acquisitions, as mainly expected for glaciers under particularly cold conditions or for structures with more stable interferometric phase such as rock glaciers or slow landslides, the Harmony formation will provide simultaneous InSAR measurements with a diversity of two (years 1 and 5) or even three (years 2–4) line-of-sight directions from one orbit, or double the amount when combining ascending and descending orbits (Figure 5).

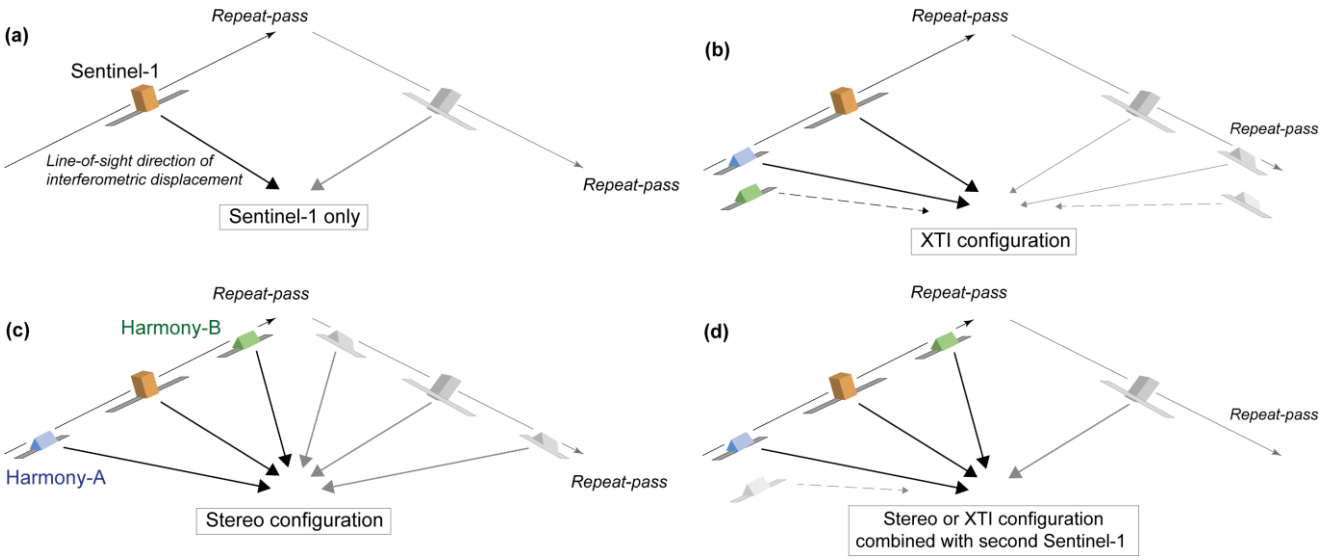


**Figure 5.** Harmony's interferometric line-of-sight diversity. (**a**) Sentinel-1 alone is able to provide radar interferometry along one line-of-sight (two if both ascending and descending orbits are combined; grey column to the right). (**b**) In XTI configuration, Harmony will provide two lines of sight (strictly speaking three, but the lines of sight of both Harmony satellites are very similar), and four if both ascending and descending orbits are combined. (**c**) In stereo configuration, Harmony will provide interferometry along three, or six, lines of sight, respectively. The three lines of sight per orbit in stereo configuration lie, though, approximately in one oblique plane. (**d**) Harmony interferograms from one orbit can also be combined with interferograms from an opposite orbit of the other Sentinel-1, providing four lines of sight.

Using traditional InSAR, one component of the displacement vector is measured (or at most two components when combining data from ascending and descending orbits) (Figure 5), achieving a geo-physically useful projection typically by assuming that the ice flows parallel to the ice surface [5,52]. This approach assumes that the ice flow is in equilibrium with the gravitational driving stress, precludes measuring any changes in surface slope and elevation that would come from changes in basal drag or sub-glacial

water distribution, and neglects vertical displacement associated with accumulation and ablation rates of the ice [51,53–55].

Full 3D measurements of ice surface velocity and deformation (Figure 5) are needed to solve these issues in order to advance ice dynamic modelling or to assess, for instance, impacts of changes in glacier drainage [55,56]. To date, such 3D data of surface displacement have been achieved either by a combination of InSAR and ice dynamic modelling or by using—rarely available—three different interferometrically coherent passes [51,53–59]. Precise 3D measurements of ice surface deformation are crucial, for instance, for understanding and quantifying processes governing glacier hydraulics, effects of subglacial volcanism, and processes leading to sub- and intra-glacial water outbreaks. Measuring three-dimensional ice surface velocity contributes to quantifying the processes involved in the specific local glacier mass balance and thickness change as a local elevation change is an effect of both surface mass balance and the vertical component of ice flow (Figure 6). Succeeding in finally gaining access to the subsidence or emergence speed components of the ice flow would thus give insight into the mean rates of accumulation and ablation. Such measurements would be highly useful to constrain regional climate models that are used, for example, to estimate and refine the input flux of ice in mass balance exercises. Strictly speaking, 3D interferometric measurements over 12-day time intervals or multiples of it will follow the phase center of the radar waves, which in the case of snow, firn, and ice might not necessarily be exactly the motion of a pack of ice crystals (Figure 6).

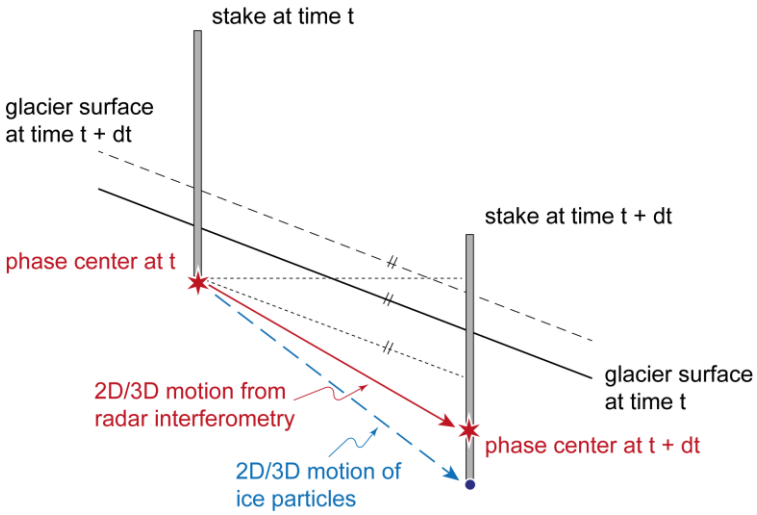


**Figure 6.** Interferometric measurements by the Harmony mission along two or more lines of sight will facilitate the measurement of three-dimensional glacier flow close to the surface. Such measurements will connect between the vertical component of ice flow, thickness changes over time, and local mass balance (i.e., directly measure components of the so-called kinematic boundary condition). Changes in the penetrated snow and firn pack could lead, though, to offsets between the true ice particle displacement and the displacement between the phase centers of the radar waves.

For small, interferometrically coherent flow rates, the Sentinel-1/Harmony formation will routinely provide 3D displacement measurements with cm-precision. As the two or three lines of sight of the formation lie actually roughly in one oblique plane, truly 3D vectors will require combining radar interferograms from ascending/descending passes. If both Sentinel-1 satellites acquire over the same area, interferograms of the other Sentinel-1 can also be applied for this purpose (Figure 5d), potentially relaxing the duration required with interferometrically coherent ground conditions, or providing additional redundancy. In any case, Harmony will add along-track interferometric sensitivity to the cross-track sensitivity that Sentinel-1 already offers. For larger, interferometrically non-coherent displacements, the combination of offset tracking between ascending and descending orbits might still be able to resolve surface flow in 3D [49,51].

### *5.2. Permafrost Ground Motion and Elevation Changes*

Radar interferometry is increasingly used to measure and monitor changes in lowland and mountain permafrost. Seasonal and multi-year subsidence and frost heave rates, typically on the order of cm/yr, are measured using repeat-pass interferometry [13,60,61]. Larger changes, such as from thaw slumps, are detected using repeat single-pass DEMs [14]. Radar interferograms are used to map mountain rock glaciers and quantify seasonal variations of rock glacier motion [3,62,63]. The Harmony mission will be able to extend these types of measurements. Two/three-dimensional surface deformations at a global scale over the planned 5-year mission lifetime will help to better understand possible lateral components of lowland permafrost deformation, for instance, in the presence of terrain gradients. The measurement accuracy of purely vertical displacements will also be enhanced due to the diversity of Harmony's lines of sight providing measurement redundancy and the associated potential to assess atmospheric influences. Measurement of rock glacier deformation has so far assumed surface-parallel motion, neglecting, for instance, rock glacier thickness changes. A combination of data from ascending and descending orbits of single radar satellites is often no option in steep mountain topography. Over its 5-year lifetime, the Harmony mission could thus make it possible to separate climatically driven changes in rock glacier ice content from dynamically caused thickness changes. The repeat interferometric single-pass DEMs during years 1 and 5 of the mission are suited to detect pronounced landscape changes such as permafrost landslides and thaw slumps, extending, for instance, time series from TanDEM-X and optical stereo data.

### *5.3. Periglacial and Paraglacial Landslides*

The mountain cryosphere and its climatically driven changes give frequently rise to peri- and paraglacial landslides [64–67]. Past and current glacier retreat and the associated de-buttressing of adjacent valley flanks, for instance, cause under certain geological circumstances large and slowly moving slope instabilities (e.g., deep-seated gravitational slope deformations; "Sackung"), a process that affects large areas in many mountain ranges and has substantial practical implications. The patterns of three-dimensional surface displacements give crucial information about the internal dynamics of such slope movements, not least about the geometry of their bedding surface, and are thus of not only large scientific but also applied importance [68–71] (Figure 7). Such three-dimensional surface kinematics can typically only be retrieved from local measurements, such as in situ geodetic measurements, photogrammetry, or local radar interferometry. At the same time, slow-moving landslides in mountain regions often show good phase coherence in satellite interferometric data. SAR interferometry is thus often used to detect and monitor such slow landslides [72,73]. Current satellite radar interferometry typically enables measurements only in one line of sight, and the method is not sensitive in orbit direction, complicating the monitoring of landslide motion in, roughly, the North–South direction [74,75]. The multiple lines of sight feasible through Harmony will facilitate the observation of landslides that move predominantly towards north or south and the measurement of two displacement components instead of one so far (Figure 7). For landslides that are visible from both ascending and descending orbit tracks, i.e., not in layover or foreshortening zones for one of these, up to six displacement components will be measured using Harmony [74]. This will finally enable, for the first time, the direct radar-interferometric measurement of three-dimensional surface motion on a large number of slow-moving landslides. Over longer coherence times, Harmony might enable highly precise measurement of two- or three-dimensional motion of persistent scatterers (PSI technique). The interferometric measurements on slow landslides can be complemented by elevation differences from Harmony's DEM stacks or other DEMs (Figure 7).

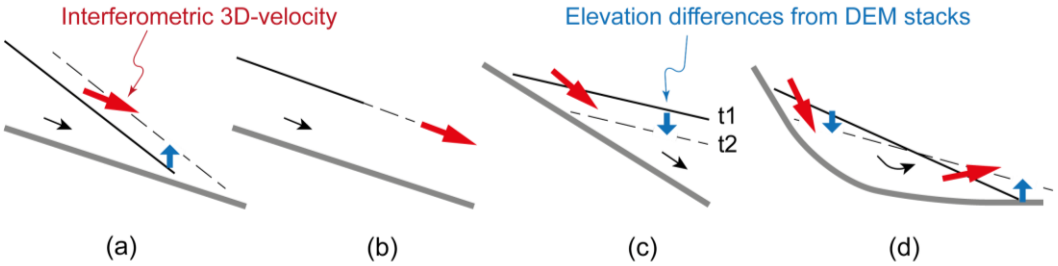


**Figure 7.** 2D schemes of different idealized cross-sections and kinematics of slow landslides. (**a**) surface slope steeper than bedding slope, (**b**) both similar, (**c**) bedding slope steeper than surface, (**d**) rotational landslide. Interferometric measurements from repeat Harmony data would enable estimating two- or three-dimensional surface velocities (red arrows). DEM stacks from Harmony's XTI phases (or other DEMs) can give elevation changes (blue arrows). Surface at time 1, black line; surface at time 2, black dashed line; bedding plane, grey line.

## 6. Multistatic Backscatter

In addition to the above nominal primary and secondary goals of the Harmony mission concerning the land cryosphere, a number of other cryosphere-related applications can be envisaged, exploiting, for instance, the unique multistatic backscatter amplitude, interferometry and polarization that Harmony provides. These potential applications need further exploration and might only develop once Harmony acquires data as no comparable data are available today. Here, we mention shortly only two of such potential cryospheric applications.

Harmony will likely be the first satellite SAR mission with large bistatic baselines of several hundred kilometers along track, i.e., a base-to-height ratio of roughly 0.5, in one (years 2–4) or two directions (years 1 and 5), and thus squint angles of up to around 25°. Bistatic backscatter under such large baselines is so far little explored [76–79]. In general, a large potential to support landcover classification is suggested, with the largest sensitivity in the specular direction [80], which Harmony will, however, not be able to cover. The largest spaceborne bistatic baselines available so far stem from TanDEM-X experiments during 2015 where cross-track baselines of several hundred meters to a few kilometers were tested, i.e., two orders of magnitude smaller base-to-height ratios than what will be available for Harmony. Stefko et al. [81] investigated in detail such TanDEM-X bi-static backscatter for Aletsch Glacier, Switzerland, and two glaciers in the Karakorum. Here, we also visually explored a few TanDEM-X acquisitions of 2015 with comparably long baselines and the associated differences between the two bistatic backscatter images. Over glaciers, we find mostly some large-scale variations, likely related to variations in snow-cover type, in particular, the existence of dry snow (see Supplement to Stefko et al. [81]) (Figure 8). It is important to note that this effect applies to coherent backscatter and is thus not directly applicable to the much larger bistatic angles for the Harmony stereo phases, but rather to the XTI phases.

As a second example, and related to the above differences between bistatic backscatter amplitudes and to the multi-directional interferometric approach to estimate radar penetration presented in Section 3.2 (second list topic), Harmony could improve possibilities to estimate the snow-water equivalent (SWE) of dry snow packs from space. By extending the theory laid out by Guneriussen et al. [9] to estimate changes in SWE through differential interferometric phase delays between repeat-pass interferograms (e.g., [82]), Harmony has the potential to overcome some of the practical limitations of the latter approach through its large diversity of line-of-sight directions [83]. The basic concept is to exploit the fact that the travel distance of the radar waves through snow will be different in the repeat-pass interferograms from Sentinel-1 and the two Harmony satellites, with the travel distance being larger for the larger along-track angles of Harmony compared to Sentinel-1. This longer travel distance translates into proportionally larger interferometric phase delays caused by the dielectric permittivity of the snow (see also second list item in Section 3.2).

The differential phase delays may be exploited to obtain absolute SWE change estimates for dry snow without the need for phase unwrapping and may provide direct estimates of the dielectric permittivity of the snow cover, hence, a proxy for the snow density [83].

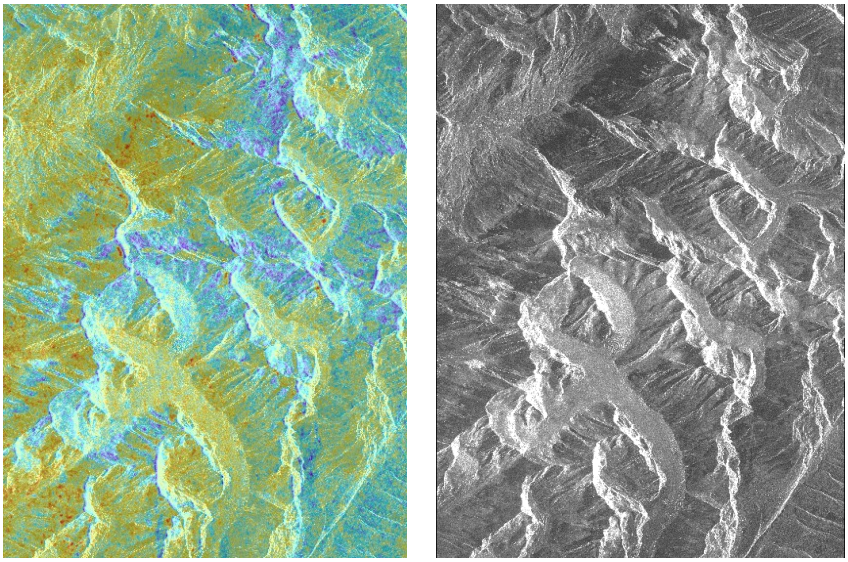

(**a**) (**b**)

**Figure 8.** (**a**) Normalized differences between the two unit-less amplitude images of a TanDEM-X bi-static acquisition of 13 April 2015 over Aletsch Glacier (**b**) and Bernese Alps, Switzerland, with approx. 500 m along-track baseline and 2 km cross-track baseline, i.e., approx. 2060 m total baseline. The noise-filtered color-coded normalized differences are transparently laid over one of the amplitude images. The more blue or red, resp., the stronger the differences are. Image in raw radar geometry, flying direction from top to bottom (descending), look direction from right to left. Strongest variations in differences between the two amplitude images are found for higher elevations, likely related to variations in snow cover type. (For other examples, see Stefko et al. [81].)

## 7. Conclusions

The ESA EarthExplorer 10 mission Harmony, a flexible constellation of two passive SAR companions to one Sentinel-1 that serves as transmitter, will deliver a number of conceptually new observations of the land cryosphere, providing a number of novel products and opportunities to explore unprecedented measurement types. Harmony will be the first mission to provide 12-day repeat DEMs over large parts of the land cryosphere for the full years 1 and 5 of the mission, useful for high-resolution global glacier volume changes and diverse studies of large and fast elevation changes in the cryosphere, such as glacier surges and permafrost thaw slumps. For Harmony's cross-track interferometric DEM generation, special attention needs to be on the estimation and correction of elevation biases due to penetration of the C-band radar waves into the snow and firn volume. For glaciers, Harmony's elevation-change time series can be combined with 12-day (or 6-day for both Sentinel-1) repeat lateral displacements from offset tracking. For interferometrically coherent ground surface conditions, Harmony can measure interferometric displacements in up to three lines of sight, and up to six if ascending and descending orbits are combined. This will give new insights into glacier and ice-sheet mass balance, and the dynamics of glacial, periglacial, and paraglacial movements by measuring, e.g., three-dimensional ice velocity. It is a particular strength of the mission to be able to, thus, measure large topographic changes and lateral displacements (scale of meters and tens of meters) through repeat cross-track interferometric elevation models and SAR offset tracking, and, at the same time, small changes (cm-scale) in three dimensions, thanks to the diversity of Harmony's SAR lines of sight. So far, little explored opportunities, for instance, for the characterization of snow properties and estimation of dry snow water equivalent, can be expected from

Harmony's multiple lines of sight and bistatic backscatter. The Harmony mission also serves a number of goals related to oceans and solid earth, requiring compromises, for instance, regarding the timing and length of the XTI and stereo phases of the mission. Harmony is designed to be able to acquire data whenever its Sentinel-1 mothership transmits and in whatever SAR mode.

**Author Contributions:** All authors contributed to the conceptualization, and writing and editing of the manuscript; figures, A.K. All authors have read and agreed to the published version of the manuscript.

**Funding:** The work was supported by European Space Agency Harmony study contracts (4000135083/21/NL/FF/ab). A.K. acknowledges also support by ESA contracts Glacier_cci and Permafrost_cci. (4000123681/18/I-NB, 4000127593/19/I-NB).

**Data Availability Statement:** Not relevant.

**Acknowledgments:** We would like to thank the ESA Advisory Committee for Earth Observation (ACEO) for their advice to the mission development, and numerous ESA-ESTEC staff for their work on the mission development. Thanks are due to two referees for their constructive comments. TerraSAR-X data for Figure 7 were obtained from DLR under proposal LAN0211. ArcticDEM data for Figure 4 are provided by the Polar Geospatial Center under NSF-OPP awards.

**Conflicts of Interest:** All authors were or are part of the ESA EarthExplorer 10 Harmony Mission Advisory Group (MAG) or involved in the associated studies. B.R. is the ESA scientific officer for the Harmony mission. Authors H.R. and T.N. conducted the work in part in contract to the company ENVEO. The remaining authors declare that the research was conducted in the absence of any commercial or financial relationships that could be construed as a potential conflict of interest. The funders had no role in the design of the study; in the collection, analyses, or interpretation of data; in the writing of the manuscript; or in the decision to publish the results.

## References

1. Rott, H. Advances in interferometric synthetic aperture radar (insar) in earth system science. *Prog. Phys. Geogr.* **2009**, *33*, 769–791. [CrossRef]
2. Strozzi, T.; Paul, F.; Wiesmann, A.; Schellenberger, T.; Kääb, A. Circum-arctic changes in the flow of glaciers and ice caps from satellite sar data between the 1990s and 2017. *Remote Sens.* **2017**, *9*, 947. [CrossRef]
3. Strozzi, T.; Caduff, R.; Jones, N.; Barboux, C.; Delaloye, R.; Bodin, X.; Kaab, A.; Matzler, E.; Schrott, L. Monitoring rock glacier kinematics with satellite synthetic aperture radar. *Remote Sens.* **2020**, *12*, 559. [CrossRef]
4. Mouginot, J.; Rignot, E.; Bjork, A.A.; van den Broeke, M.; Millan, R.; Morlighem, M.; Noël, B.; Scheuchl, B.; Wood, M. Forty-six years of greenland ice sheet mass balance from 1972 to 2018. *Proc. Natl. Acad. Sci. USA* **2019**, *116*, 9239–9244. [CrossRef] [PubMed]
5. Mouginot, J.; Rignot, E.; Scheuchl, B. Continent-wide, interferometric sar phase, mapping of antarctic ice velocity. *Geophys. Res. Lett.* **2019**, *46*, 9710–9718. [CrossRef]
6. Friedl, P.; Weiser, F.; Fluhrer, A.; Braun, M.H. Remote sensing of glacier and ice sheet grounding lines: A review. *Earth-Sci. Rev.* **2020**, *201*, 102948. [CrossRef]
7. Bhattacharjee, S.; Garg, R.D. Estimation of sea ice drift and concentration during melt season using c-band dual-polarimetric sentinel-1 data. *Remote Sens. Appl.* **2024**, *33*, 101104. [CrossRef]
8. Dammann, D.O.; Eicken, H.; Meyer, F.J.; Mahoney, A.R. Assessing small-scale deformation and stability of landfast sea ice on seasonal timescales through l-band sar interferometry and inverse modeling. *Remote Sens. Environ.* **2016**, *187*, 492–504. [CrossRef]
9. Guneriussen, T.; Hogda, K.A.; Johnsen, H.; Lauknes, I. Insar for estimation of changes in snow water equivalent of dry snow. *IEEE Trans. Geosci. Remote* **2001**, *39*, 2101–2108. [CrossRef]
10. Nagler, T.; Rott, H.; Ripper, E.; Bippus, G.; Hetzenecker, M. Advancements for snowmelt monitoring by means of sentinel-1 sar. *Remote Sens.* **2016**, *8*, 348. [CrossRef]
11. Lievens, H.; Brangers, I.; Marshall, H.P.; Jonas, T.; Olefs, M.; De Lannoy, G. Sentinel-1 snow depth retrieval at sub-kilometer resolution over the european alps. *Cryosphere* **2022**, *16*, 159–177. [CrossRef]
12. Lund, J.; Forster, R.R.; Deeb, E.J.; Liston, G.E.; Skiles, S.M.; Marshall, H.P. Interpreting sentinel-1 sar backscatter signals of snowpack surface melt/freeze, warming, and ripening, through field measurements and physically-based snowmodel. *Remote Sens.* **2022**, *14*, 4002. [CrossRef]
13. Strozzi, T.; Antonova, S.; Gunther, F.; Matzler, E.; Vieira, G.; Wegmuller, U.; Westermann, S.; Bartsch, A. Sentinel-1 sar interferometry for surface deformation monitoring in low-land permafrost areas. *Remote Sens.* **2018**, *10*, 1360. [CrossRef]
14. Bernhard, P.; Zwieback, S.; Leinss, S.; Hajnsek, I. Mapping retrogressive thaw slumps using single-pass tandem-x observations. *IEEE J.-Stars.* **2020**, *13*, 3263–3280. [CrossRef]

15. López-Dekker, P.; Krieger, G.; Moreira, A. Multistatic radar systems. In *Distributed Space Missions for Earth System Monitoring*; D'Errico, M., Ed.; Springer: New York, NY, USA, 2013; pp. 61–122.
16. Van Zyl, J.J. The shuttle radar topography mission (srtm): A breakthrough in remote sensing of topography. *Acta Astronaut.* **2001**, *48*, 559–565. [CrossRef]
17. Zink, M.; Moreira, A.; Hajnsek, I.; Rizzoli, P.; Bachmann, M.; Kahle, R.; Fritz, T.; Huber, M.; Krieger, G.; Lachaise, M.; et al. Tandem-x: 10 years of formation flying bistatic sar interferometry. *IEEE J.-Stars.* **2021**, *14*, 3546–3565. [CrossRef]
18. ESA. *Report for Mission Selection: Earth Explorer 10 Candidate Mission Harmony*; ESA: Noordwijk, The Netherlands, 2022; p. 369.
19. ESA. *Esa's Living Planet Programme: Scientific Achievements and Future Challenges—Scientific Context of the Earth Observation Science Strategy for Esa (esa sp-1329/2, February 2015)*; ESA: Noordwijk, The Netherlands, 2015; p. 67.
20. Theodosiou, A.; Kleinherenbrink, M.; López-Dekker, P. Wide-swath ocean altimetry using multisatellite single-pass interferometry. *IEEE Trans. Geosci. Remote* **2023**, *61*, 5210721. [CrossRef]
21. Kleinherenbrink, M.; Korosov, A.; Newman, T.; Theodosiou, A.; Komarov, A.S.; Li, Y.H.; Mulder, G.; Rampal, P.; Stroeve, J.; Lopez-Dekker, P. Estimating instantaneous sea-ice dynamics from space using the bi-static radar measurements of earth explorer 10 candidate harmony. *Cryosphere* **2021**, *15*, 3101–3118. [CrossRef]
22. Berthier, E.; Floriciou, D.; Gardner, A.S.; Gourmelen, N.; Jakob, L.; Paul, F.; Treichler, D.; Wouters, B.; Belart, J.M.C.; Dehecq, A.; et al. Measuring glacier mass changes from space—A review. *Rep. Prog. Phys.* **2023**, *86*, 036801. [CrossRef]
23. Zemp, M.; Huss, M.; Thibert, E.; Eckert, N.; McNabb, R.; Huber, J.; Barandun, M.; Machguth, H.; Nussbaumer, S.U.; Gartner-Roer, I.; et al. Global glacier mass changes and their contributions to sea-level rise from 1961 to 2016. *Nature* **2019**, *568*, 382–386.
24. Hugonnet, R.; McNabb, R.; Berthier, E.; Menounos, B.; Nuth, C.; Girod, L.; Farinotti, D.; Huss, M.; Dussaillant, I.; Brun, F.; et al. Accelerated global glacier mass loss in the early twenty-first century. *Nature* **2021**, *592*, 726–731. [CrossRef] [PubMed]
25. Kääb, A.; Berthier, E.; Nuth, C.; Gardelle, J.; Arnaud, Y. Contrasting patterns of early twenty-first-century glacier mass change in the himalayas. *Nature* **2012**, *488*, 495–498. [CrossRef] [PubMed]
26. McMillan, M.; Shepherd, A.; Muir, A.; Gaudelli, J.; Hogg, A.E.; Cullen, R. Assessment of cryosat-2 interferometric and non-interferometric sar altimetry over ice sheets. *Adv. Space Res.* **2018**, *62*, 1281–1291. [CrossRef]
27. Morris, A.; Moholdt, G.; Gray, L. Spread of svalbard glacier mass loss to barents sea margins revealed by cryosat-2. *J. Geophys. Res.-Earth* **2020**, *125*, e2019JF005357. [CrossRef]
28. Jakob, L.; Gourmelen, N.; Ewart, M.; Plummer, S. Spatially and temporally resolved ice loss in high mountain asia and the gulf of alaska observed by cryosat-2 swath altimetry between 2010 and 2019. *Cryosphere* **2021**, *15*, 1845–1862. [CrossRef]
29. Porter, C.; Howat, I.; Noh, M.-J.; Husby, E.; Khuvis, S.; Danish, E.; Tomko, K.; Gardiner, J.; Negrete, A.; Yadav, B.; et al. *Arcticdem—Strips, Version 4.1*, 6th ed.; Polar Geospatial, C., Ed.; Harvard Dataverse: Cambridge, MA, USA, 2022.
30. Dall, J.; Madsen, S.N.; Keller, K.; Forsberg, R. Topography and penetration of the greenland ice sheet measured with airborne sar interferometry. *Geophys. Res. Lett.* **2001**, *28*, 1703–1706. [CrossRef]
31. Rignot, E.; Echelmeyer, K.; Krabill, W. Penetration depth of interferometric synthetic-aperture radar signals in snow and ice. *Geophys. Res. Lett.* **2001**, *28*, 3501–3504. [CrossRef]
32. Gardelle, J.; Berthier, E.; Arnaud, Y. Impact of resolution and radar penetration on glacier elevation changes computed from multi-temporal dems. *J. Glaciol.* **2012**, *58*, 419–422. [CrossRef]
33. Rott, H.; Scheiblauer, S.; Wuite, J.; Krieger, L.; Floricioiu, D.; Rizzoli, P.; Libert, L.; Nagler, T. Penetration of interferometric radar signals in antarctic snow. *Cryosphere* **2021**, *15*, 4399–4419. [CrossRef]
34. Benedikter, A.; Rodriguez-Cassola, M.; Prats-Iraola, P.; Krieger, G.; Fischer, G. On the processing of single-pass insar data for accurate elevation measurements of ice sheets and glaciers. *IEEE Trans. Geosci. Remote* **2024**, *62*, 4300310. [CrossRef]
35. Dall, J. Insar elevation bias caused by penetration into uniform volumes. *IEEE Trans. Geosci. Remote* **2007**, *45*, 2319–2324. [CrossRef]
36. Nolan, M.; Larsen, C.; Sturm, M. Mapping snow depth from manned aircraft on landscape scales at centimeter resolution using structure-from-motion photogrammetry. *Cryosphere* **2015**, *9*, 1445–1463. [CrossRef]
37. Treichler, D.; Kaab, A. Snow depth from icesat laser altimetry—A test study in southern norway. *Remote Sens. Environ.* **2017**, *191*, 389–401. [CrossRef]
38. Deschamps-Berger, C.; Gascoin, S.; Berthier, E.; Deems, J.; Gutmann, E.; Dehecq, A.; Shean, D.; Dumont, M. Snow depth mapping from stereo satellite imagery in mountainous terrain: Evaluation using airborne laser-scanning data. *Cryosphere* **2020**, *14*, 2925–2940. [CrossRef]
39. Kääb, A.; Leinss, S.; Gilbert, A.; Buhler, Y.; Gascoin, S.; Evans, S.G.; Bartelt, P.; Berthier, E.; Brun, F.; Chao, W.A.; et al. Massive collapse of two glaciers in western tibet in 2016 after surge-like instability. *Nat. Geosci.* **2018**, *11*, 114–120. [CrossRef]
40. Kääb, A.; Jacquemart, M.; Gilbert, A.; Leinss, S.; Girod, L.; Huggel, C.; Falaschi, D.; Ugalde, F.; Petrakov, D.; Chernomorets, S.; et al. Sudden large-volume detachments of low-angle mountain glaciers. More frequent than thought? *Cryosphere* **2021**, *15*, 1751–1785. [CrossRef]
41. Guillet, G.; King, O.; Lv, M.Y.; Ghuffar, S.; Benn, D.; Quincey, D.; Bolch, T. A regionally resolved inventory of high mountain asia surge-type glaciers, derived from a multi-factor remote sensing approach. *Cryosphere* **2022**, *16*, 603–623. [CrossRef]
42. Kääb, A.; Girod, L. Brief communication: Rapid $\sim$ 335 x 10m bed erosionafter detachment of the sedongpu glacier (tibet). *Cryosphere* **2023**, *17*, 2533–2541. [CrossRef]
43. Joughin, I.; Shean, D.E.; Smith, B.E.; Floricioiu, D. A decade of variability on jakobshavn isbrae: Ocean temperatures pace speed through influence on melange rigidity. *Cryosphere* **2020**, *14*, 211–227. [CrossRef]

44. Mouginot, J.; Rignot, E.; Scheuchl, B. Sustained increase in ice discharge fromthe amundsen sea embayment, west antarctica, from1973 to 2013. *Geophys. Res. Lett.* **2014**, *41*, 1576–1584. [CrossRef]
45. Mankoff, K.D.; Colgan, W.; Solgaard, A.; Karlsson, N.B.; Ahlstrom, A.P.; van As, D.; Box, J.E.; Khan, S.A.; Kjeldsen, K.K.; Mouginot, J.; et al. Greenland ice sheet solid ice discharge from 1986 through 2017. *Earth Syst. Sci. Data* **2019**, *11*, 769–786. [CrossRef]
46. Rignot, E.; Mouginot, J.; Scheuchl, B.; van den Broeke, M.; van Wessem, M.J.; Morlighem, M. Four decades of antarctic ice sheet mass balance from 1979–2017. *Proc. Natl. Acad. Sci. USA* **2019**, *116*, 1095–1103. [CrossRef] [PubMed]
47. King, M.D.; Howat, I.M.; Candela, S.G.; Noh, M.J.; Jeong, S.; Noël, B.P.Y.; van den Broeke, M.R.; Wouters, B.; Negrete, A. Dynamic ice loss from the greenland ice sheet driven by sustained glacier retreat. *Commun. Earth Environ.* **2020**, *1*, 1. [CrossRef]
48. Wendt, A.; Mayer, C.; Lambrecht, A.; Floricioiu, D. A glacier surge of bivachny glacier, pamir mountains, observed by a time series of high-resolution digital elevation models and glacier velocities. *Remote Sens.* **2017**, *9*, 388. [CrossRef]
49. Samsonov, S.; Tiampo, K.; Cassotto, R. Sar-derived flow velocity and its link to glacier surface elevation change and mass balance. *Remote Sens. Environ.* **2021**, *258*, 112343. [CrossRef]
50. Samsonov, S.; Tiampo, K.; Cassotto, R. Measuring the state and temporal evolution of glaciers in alaska and yukon using synthetic-aperture-radar-derived (sar-derived) 3d time series of glacier surface flow. *Cryosphere* **2021**, *15*, 4221–4239. [CrossRef]
51. Nagler, T.; Rott, H.; Hetzenecker, M.; Scharrer, K.; Magnússon, E.; Floricioiu, D.; Notarnicola, C. Retrieval of 3d-glacier movement by high resolution x-band sar data. In Proceedings of the 2012 IEEE International Geoscience and Remote Sensing Symposium, Munich, Germany, 22–27 July 2012; pp. 3233–3236.
52. Joughin, I.R.; Kwok, R.; Fahnestock, M.A. Interferometric estimation of three-dimensional ice-flow using ascending and descending passes. *IEEE Trans. Geosci. Remote* **1998**, *36*, 25–37. [CrossRef]
53. Gray, L. Using multiple radarsat insar pairs to estimate a full three-dimensional solution for glacial ice movement. *Geophys. Res. Lett.* **2011**, *38*, L05502. [CrossRef]
54. Andersen, J.K.; Rathmann, N.; Hvidberg, C.S.; Grinsted, A.; Kusk, A.; Boncori, J.P.M.; Mouginot, J. Episodic subglacial drainage cascades below the northeast greenland ice stream. *Geophys. Res. Lett.* **2023**, *50*, e2023GL103240. [CrossRef]
55. Maier, N.; Andersen, J.K.; Mouginot, J.; Gimbert, F.; Gagliardini, O. Wintertime supraglacial lake drainage cascade triggers large-scale ice flow response in greenland. *Geophys. Res. Lett.* **2023**, *50*, e2022GL102251. [CrossRef]
56. Magnússon, E.; Björnsson, H.; Rott, H.; Pálsson, F. Reduced glacier sliding caused by persistent drainage from a subglacial lake. *Cryosphere* **2010**, *4*, 13–20. [CrossRef]
57. Reeh, N.; Mohr, J.J.; Madsen, S.N.; Oerter, H.; Gundestrup, N.S. Three-dimensional surface velocities of storstrommen glacier, greenland, derived from radar interferometry and ice-sounding radar measurements. *J. Glaciol.* **2003**, *49*, 201–209. [CrossRef]
58. Gudmundsson, S.; Sigmundsson, F.; Carstensen, J.M. Three-dimensional surface motion maps estimated from combined interferometric synthetic aperture radar and gps data. *J. Geophys. Res.-Solid. Earth* **2002**, *107*, 2250. [CrossRef]
59. Magnússon, E.; Rott, H.; Björnsson, H.; Pálsson, F. The impact of jokulhlaups on basal sliding observed by sar interferometry on vatnajokull, iceland. *J. Glaciol.* **2007**, *53*, 232–240. [CrossRef]
60. Schaefer, K.; Liu, L.; Parsekian, A.; Jafarov, E.; Chen, A.; Zhang, T.J.; Gusmeroli, A.; Panda, S.; Zebker, H.A.; Schaefer, T. Remotely sensed active layer thickness (resalt) at barrow, alaska using interferometric synthetic aperture radar. *Remote Sens.* **2015**, *7*, 3735–3759. [CrossRef]
61. Rouyet, L.; Lauknes, T.R.; Christiansen, H.H.; Strand, S.M.; Larsen, Y. Seasonal dynamics of a permafrost landscape, adventdalen, svalbard, investigated by insar. *Remote Sens. Environ.* **2019**, *231*, 111236. [CrossRef]
62. Kääb, A.; Strozzi, T.; Bolch, T.; Caduff, R.; Trefall, H.; Stoffel, M.; Kokarev, A. Inventory and changes of rock glacier creep speeds in ile alatau and kungöy ala-too, northern tien shan, since the 1950s. *Cryosphere* **2021**, *15*, 927–949. [CrossRef]
63. Bertone, A.; Barboux, C.; Bodin, X.; Bolch, T.; Brardinoni, F.; Caduff, R.; Christiansen, H.H.; Darrow, M.M.; Delaloye, R.; Etzelmüller, B.; et al. Incorporating insar kinematics into rock glacier inventories: Insights from 11 regions worldwide. *Cryosphere* **2022**, *16*, 2769–2792. [CrossRef]
64. Ballantyne, C.K. Paraglacial geomorphology. *Quat. Sci. Rev.* **2002**, *21*, 1935–2017. [CrossRef]
65. Kääb, A. Remote sensing of permafrost-related problems and hazards. *Permafr. Periglac.* **2008**, *19*, 107–136. [CrossRef]
66. McColl, S.T. Paraglacial rock-slope stability. *Geomorphology* **2012**, *153*, 1–16. [CrossRef]
67. Cossart, É.; Mercier, D.; Decaulne, A.; Feuillet, T. An overview of the consequences of paraglacial landsliding on deglaciated mountain slopes: Typology, timing and contribution to cascading fluxes. *Quaternaire* **2013**, *24*, 13–24. [CrossRef]
68. Kos, A.; Amann, F.; Strozzi, T.; Delaloye, R.; von Ruette, J.; Springman, S. Contemporary glacier retreat triggers a rapid landslide response, great aletsch glacier, switzerland. *Geophys. Res. Lett.* **2016**, *43*, 12466–12474. [CrossRef]
69. Kääb, A. *Remote Sensing of Mountain Glaciers and Permafrost Creep*; University of Zurich: Zurich, Switzerland, 2005; Volume 48, p. 266.
70. Strozzi, T.; Delaloye, R.; Kääb, A.; Ambrosi, C.; Perruchoud, E.; Wegmüller, U. Combined observations of rock mass movements using satellite sar interferometry, differential gps, airborne digital photogrammetry, and airborne photography interpretation. *J. Geophys. Res.-Earth* **2010**, *115*, F01014. [CrossRef]
71. Raucoules, D.; de Michele, M.; Malet, J.P.; Ulrich, P. Time-variable 3d ground displacements from high-resolution synthetic aperture radar (sar). Application to la valette landslide (south french alps). *Remote Sens. Environ.* **2013**, *139*, 198–204. [CrossRef]
72. Strozzi, T.; Ambrosi, C.; Raetzo, H. Interpretation of aerial photographs and satellite sar interferometry for the inventory of landslides. *Remote Sens.* **2013**, *5*, 2554–2570. [CrossRef]

73. Strozzi, T.; Raetzo, H.; Wegmuller, U.; Papke, J.; Caduff, R.; Werner, C.; Wiesmann, A. Satellite and terrestrial radar interferometry for the measurement of slope deformation. In *Engineering Geology for Society and Territory—Volume 5*; Springer: Cham, Switzerland, 2015; pp. 161–165.
74. Samsonov, S.; Dille, A.; Dewitte, O.; Kervyn, F.; d'Oreye, N. Satellite interferometry for mapping surface deformation time series in one, two and three dimensions: A new method illustrated on a slow-moving landslide. *Eng. Geol.* **2020**, *266*, 105471. [CrossRef]
75. Fuhrmann, T.; Garthwaite, M.C. Resolving three-dimensional surface motion with insar: Constraints from multi-geometry data fusion. *Remote Sens.* **2019**, *11*, 241. [CrossRef]
76. Renga, A.; Gigantino, A.; Graziano, M.D.; Moccia, A.; Fedele, A.; Natalucci, S. Design considerations and performance analysis for rodio distributed sar mission. *Acta Astronaut.* **2023**, *210*, 474–482. [CrossRef]
77. Gigantino, A.; Renga, A.; Graziano, M.D.; Abbundo, C.; Ravellino, F.; Moccia, A.; di Martire, D.; Khalili, M.A.; Ramondini, M.; Pisacane, V.; et al. Long-baseline multistatic and bistatic sar products: Application to the rodio mission. *Acta Astronaut.* **2024**, *222*, 314–324. [CrossRef]
78. Bordoni, F.; Younis, M.; Rodriguez-Cassola, M.; Prats-Iraola, P.; López-Dekker, P.; Krieger, G. Saocom-cs sar imaging performance evaluation in large baseline bistatic configuration. In Proceedings of the 2015 IEEE International Geoscience and Remote Sensing Symposium (IGARSS), Milan, Italy, 26–31 July 2015; pp. 2107–2110.
79. Dubois-Fernandez, P.; Cantalloube, H.; Vaizan, B.; Krieger, G.; Horn, R.; Wendler, M.; Giroux, V. Onera-dlr bistatic sar campaign: Planning, data acquisition, and first analysis of bistatic scattering behaviour of natural and urban targets. *IEE Proc.-Radar Sonar Navig.* **2006**, *153*, 214–223. [CrossRef]
80. Pierdicca, N.; Brogioni, M.; Fascetti, F.; Ouellette, J.D.; Guerriero, L. Retrieval of biogeophysical parameters from bistatic observations of land at l-band: A theoretical study. *IEEE Trans. Geosci. Remote* **2022**, *60*, 4402517. [CrossRef]
81. Stefko, M.; Leinss, S.; Frey, O.; Hajnsek, I. Coherent backscatter enhancement in bistatic ku- and x-band radar observations of dry snow. *Cryosphere* **2022**, *16*, 2859–2879. [CrossRef]
82. Deeb, E.J.; Forster, R.R.; Kane, D.L. Monitoring snowpack evolution using interferometric synthetic aperture radar on the north slope of alaska, USA. *Int. J. Remote Sens.* **2011**, *32*, 3985–4003. [CrossRef]
83. Benedikter, A.; Belinska, K.; Rodriguez-Cassola, M.; Prats-Iraola, P.; Fischer, G.; Krieger, G.; Hajnsek, I. Towards dry snow parameter estimation by simultaneous multiple squint differential INSAR. *IEEE Trans. Geosci. Remote.* 2024, *in press*.